

# Bridging the Scales via Personalized Cellular Modeling and Deep Phenotyping in Schizophrenia

Florian J. Raabe, MD, PhD; David Popovic, MD, PhD; Clara Vetter, MS; Laura E. Fischer, MD; Genc Hasanaj, MS; Berkhan Karshi, MS; Tim J. Schäfer, MS; Valeria Almeida, PhD; Alessia Atella, MS; Miriam Gagliardi, PhD; Emanuel Boudriot, MD; Vladislav Yakimov, MD; Lucia Trastulla, PhD; Tengjia Jiang, MS; Clara Weyer, MS; Lukasz Roell, PhD; Joanna Moussiopoulou, MD; Lenka Krčmář, MD, PhD; Sabrina Galinski, PhD; Irina Papazova, PhD; Oliver Pogarell, PhD; Alkomiet Hasan, MD; Eva C. Schulte, MD, PhD; Andrea Schmitt, MD; Nikolaos Koutsouleris, MD; Anna Levina, PhD; Elias Wagner, MD; Moritz J. Rossner, PhD; Sergi Papiol, PhD; Peter Falkai, MD; Daniel Keeser, PhD; Michael J. Ziller, PhD; for the CDP Working Group

[+ Supplemental content](#)

**IMPORTANCE** While growing evidence implicates synaptic dysfunction as a key pathophysiological mechanism in cognitive impairments in schizophrenia (SCZ), it remains unknown how individual alterations in synaptic connectivity translate into corresponding neural circuit dysfunction and cognitive deficits.

**OBJECTIVE** To test whether genetically driven variability in excitatory neurons' transcriptome and synapse density in patient-derived neurons in vitro explain individual changes in cortical morphology, electrophysiology, and cognitive impairments in vivo.

**DESIGN, SETTING, AND PARTICIPANTS** This multimodal case-control study integrated deep clinical phenotyping (magnetic resonance imaging, electroencephalography, and cognitive assessments) across 2 independent cohorts with schizophrenia and healthy controls (N = 461) with donor-matched induced pluripotent stem cell (iPSC)-derived neurons (n = 80). Machine learning, transcriptome imputation, and reverse dynamic causal modeling were applied to link cellular and systems-level phenotypes. Data were collected between September 16, 2014, and November 10, 2023, and analyzed from January 2022 to January 2026.

**MAIN OUTCOMES AND MEASURES** The primary outcome was associations between cellular phenotypes (gene expression, synapse density) and individual-level brain structure, electrophysiology, and cognition.

**RESULTS** This multiscale translational framework was implemented in 461 individuals with SCZ and healthy controls across 2 independent cohorts. In both cohorts (cohort 1 [C1]: mean [SD] age: 35.1 [11.6] years; 46 female participants [31.1%]; cohort 2 [C2]: mean [SD] age, 36.9 [11.7] years; 140 female participants [44.57%]), cognitive impairments in SCZ were associated with specific gray matter volume reductions across multiple brain regions, in particular the right dorsolateral prefrontal cortex, as well as disturbed electrophysiological activity in the gamma band. Importantly, the individual-level differences in the genetically driven neuronal gene expression patterns and synapse density in vitro predicted the macro-scale alterations of brain structural (C1:  $r = 0.39$ ; 95% CI, 0.21-0.55;  $P < .001$ ; iPSC:  $r = 0.31$ ; 95% CI, -0.07 to 0.60;  $P = .049$ ; C2:  $r = 0.23$ ; 95% CI, 0.07-0.37;  $P = .003$ ), electrophysiological (theta:  $r = 0.19$ ; 95% CI, 0.04-0.32;  $P = .05$ ; gamma1:  $r = 0.17$ ; 95% CI, 0.028-0.31;  $P = .005$ ; gamma2:  $r = 0.22$ ; 95% CI, 0.07-0.35;  $P < .001$ ), and cognitive (C1:  $r = 0.76$ ; 95% CI, 0.66-0.83;  $P < .001$ ; iPSC:  $r = 0.77$ ; 95% CI, 0.57-0.89;  $P < .001$ ; C2:  $r = 0.17$ ; 95% CI, 0.02-0.32;  $P = .02$ ) phenotypes in vivo, providing a mechanistic link from synapse deficits to cognitive impairments in SCZ.

**CONCLUSIONS AND RELEVANCE** These findings establish a patient-specific link between genetically driven alterations in gene expression, synaptic dysfunction, and large-scale brain and cognitive phenotypes in SCZ. This multiscale framework provides a foundation for mechanism-based stratification and precision target identification for cognitive impairment.

**Author Affiliations:** Author affiliations are listed at the end of this article.

**Group Information:** The CDP Working Group investigators and coordinators appear in Supplement 3.

**Corresponding Author:** Florian J. Raabe, MD, PhD, Max Planck Institute of Psychiatry, Kraepelinstr. 2-10, 80804 Munich, Germany ([florian\\_raabe@psych.mpg.de](mailto:florian_raabe@psych.mpg.de)); Michael J. Ziller, PhD, Department of Psychiatry, University of Münster, 48149 Münster, Germany ([ziller@uni-muenster.de](mailto:ziller@uni-muenster.de)).

JAMA Psychiatry. 2026;83(5):510-522. doi:10.1001/jamapsychiatry.2026.0576  
Published online March 28, 2026.

Converging evidence suggests that cognitive deficits in schizophrenia (SCZ) originate in part from synaptic dysfunction, arising from a combination of genetic and environmentally triggered mechanisms,<sup>1-4</sup> which disrupt micro- and macro-connectivity of brain circuits.<sup>1</sup> Genome-wide association studies (GWAS) have identified dozens of risk genes involved in synaptic function and neurotransmission.<sup>4</sup> Moreover, meta-analyses consistently demonstrate structural gray matter volume (GMV) reductions across multiple brain regions, including the dorsolateral prefrontal cortex (DLPFC), in individuals with SCZ.<sup>5-9</sup> Importantly, postmortem and animal studies indicate that GMV changes primarily approximate reductions in dendritic volume and synaptic density.<sup>1,10-12</sup> Conversely, electroencephalography (EEG) studies in SCZ revealed aberrant theta and gamma frequency bands,<sup>13,14</sup> reflecting disrupted neural synchrony, which is linked to the disorder's characteristic cognitive deficits in working memory, attention, and executive function.<sup>14</sup>

However, despite insights across multiple scales, these findings have remained largely disconnected, and the association of intermediate phenotypes with underlying neurobiological mechanisms remains elusive.

Personalized disease models-based induced pluripotent stem cells (iPSCs) offer a pivotal technology to dissect disease-relevant molecular mechanisms in SCZ in vitro.<sup>15-17</sup> These models capture the entire (poly)genetic risk profile of their donors and allow assessment of their joint molecular and cellular effects in disease-relevant cell types.<sup>15</sup> We recently identified alternative polyadenylation as one genetically driven mechanism causing a reduction of synaptic density in iPSC-derived neurons in SCZ, independent of microglial pruning.<sup>18</sup> Most importantly, iPSCs provide the unique opportunity to link microscale molecular and cellular level changes with macroscale intermediate phenotypes.<sup>19,20</sup> Establishing such links would position iPSC technology as a powerful bridge for personalized and target-based interventions in SCZ.<sup>21</sup>

Here, we present a translational research framework designed to integrate molecular, cellular, and systems-level macrocircuit variability to uncover the neurobiological underpinnings of cognitive impairments in SCZ. Specifically, we combined deep multimodal phenotyping—including magnetic resonance imaging (MRI), EEG, and neurocognitive assessments across 2 independent cohorts<sup>20,22</sup>—with molecularly characterized iPSC-derived neurons from overlapping donors,<sup>18</sup> machine learning prediction of genetically regulated transcriptomes, and reverse personalized dynamic-causal modeling (rpDCM). This unique multiscale approach enabled us to test whether genetically driven cell-autonomous variability in excitatory neurones and synapses accounts for individual differences in cortical structure, electrophysiology, and cognitive performance (Figure 1A).

## Methods

### Participants and Study Design

This study integrates 2 independent and deeply phenotyped cross-sectional SCZ cohorts<sup>20,22</sup> (N = 461) with overlapping

### Key Points

**Question** Do synaptic deficits in patient-derived neurons predict individual differences in brain circuitry and cognitive impairment in schizophrenia (SCZ)?

**Finding** In a multiscale framework integrating magnetic resonance imaging, electroencephalography, and cognitive data from more than 500 participants with in vitro phenotyping of donor-matched induced pluripotent stem cell (iPSC)-derived neurons, reduced excitatory synapse density and transcriptomic signatures predicted the individual alterations in brain structure, electrophysiology, and cognition in vivo, providing a mechanistic link from synapse deficits to cognitive impairments in SCZ.

**Meaning** This study establishes a patient-specific bridge from synapse biology to the individual clinical phenotype, offering a road map for mechanism-based target and drug discovery.

donors from an iPSC cohort<sup>18</sup> (n = 80) (Figure 1A), both approved by the local ethics committee of Faculty of Medicine, Ludwig-Maximilians-Universität (LMU) Munich according to the principles of the Declaration of Helsinki. The included patients with SCZ spectrum disorders and healthy controls (HC), with a subset of unaffected first-degree relatives, provided written informed consent. Cognitive domains were assessed using standardized instruments encompassing verbal memory, working memory, information processing, cognitive flexibility, and crystalline intelligence.<sup>23</sup> Antipsychotic doses were harmonized using chlorpromazine equivalents (CPZeq<sup>24</sup>; details in the eMethods in Supplement 1). Study C2 was registered in the German Clinical Trials Register (DRKS, identifier DRKS00024177).

### MRI and EEG

Structural T1-weighted images were acquired from 3T MRI scans and processed using the CAT12 toolbox. GMV was analyzed on a whole-brain voxelwise (2-mm<sup>3</sup> voxel size) basis. Resting-state EEG (rsEEG) was recorded for 10 minutes using a 32-channel system with Cz as the reference electrode. Power spectral density (PSD) features were computed to extract absolute and relative power<sup>25</sup> of the different frequency bands: delta (1-4 Hz), theta (4-8 Hz), alpha (8-12 Hz), beta (12-30 Hz), gamma1 (30-50 Hz), and gamma2 (50-70 Hz). For further details, see the eMethods in Supplement 1.

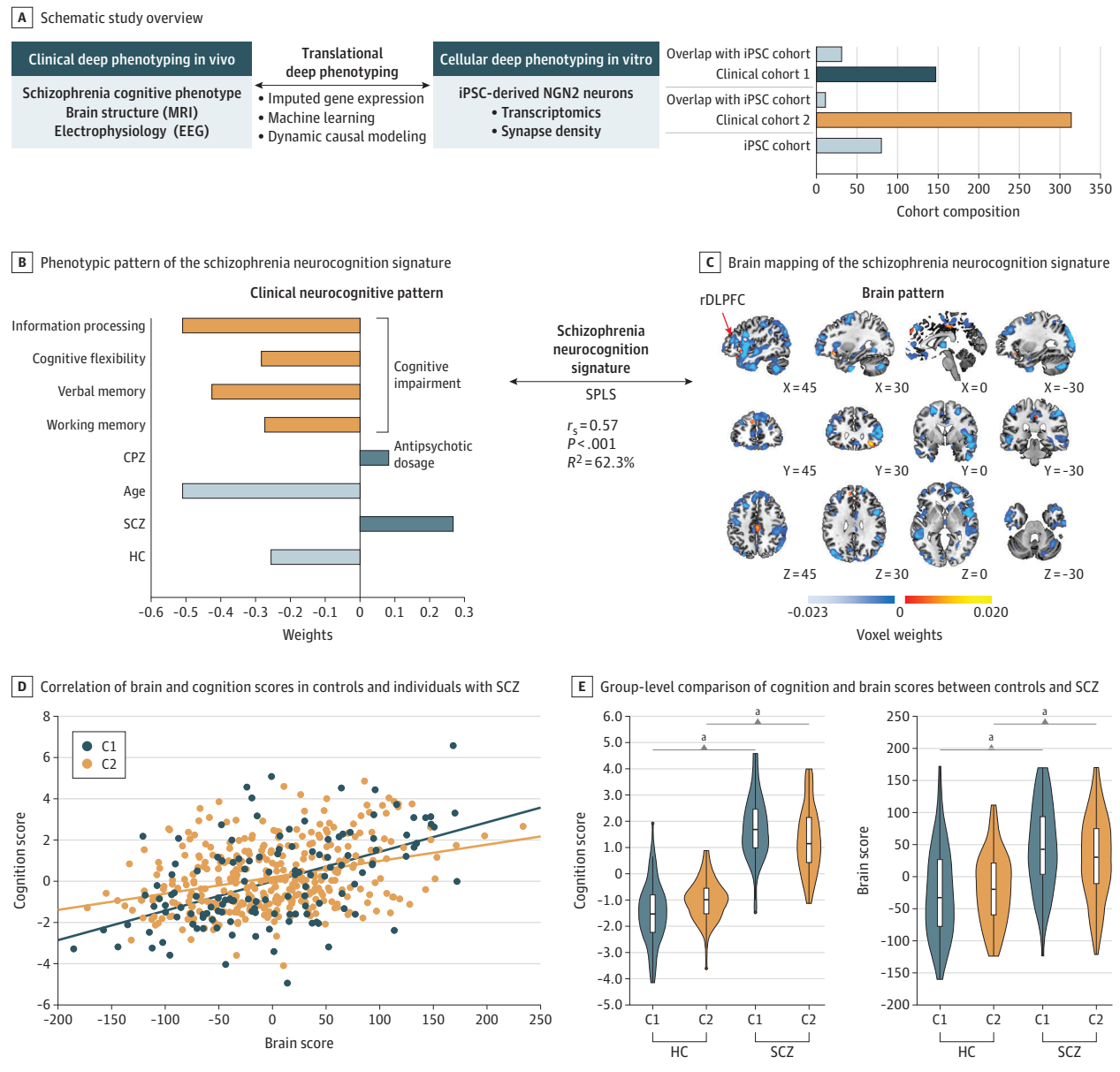
### iPSC-Derived Neurons

Induced differentiation of iPSC-derived excitatory pyramidal neurons (iNs) from the 80 donors included for this study was carried out as described previously.<sup>18</sup> For details of neuronal differentiation, technical quality control analysis, RNA-Seq data processing and analysis, imaging, and synapse density analysis, see the eMethods in Supplement 1 and supplements of our companion study.<sup>18</sup>

### Polygenic Risk Scores and Imputed Gene Expression

To calculate SCZ polygenic risk scores (SCZ-PRS) based on PGC3 GWAS,<sup>4</sup> single-nucleotide polymorphism (SNP) effect sizes were estimated using PRS-continuous shrinkage (PRS-CS).<sup>26</sup>

**Figure 1. Translational Deep Phenotyping Reveals a Multivariate Phenotype Brain Signature of Cognitive Impairments in Schizophrenia (SCZ) That Is Associated With the Genetic Risk**



A, Schematic study overview with bar plot illustrates the study design of 2 deep phenotyped cohorts 1 (C1, dark blue) and 2 (C2, orange)<sup>20</sup> that overlaps with an induced pluripotent stem cell (iPSC) cohort<sup>18</sup> (light blue) to bridge the translational gap between genetic, molecular, and cellular alterations in vitro and the in vivo individual intermediate phenotype of cognitive impairment in individuals with SCZ. B, Bar plot visualizing the phenotypic pattern of the schizophrenia neurocognition signature captured by the multivariate sparse partial least-squares (SPLS) analysis in the discovery cohort C1. The arrow indicates the Spearman coefficient ( $r$ ) and associated  $P$  value as well as the coefficient of determination ( $R^2$ ) between the cognition pattern and the brain pattern within the signature ( $n = 131$ ;  $r = 0.57$ ;  $P < .001$ ,  $t$  test;  $R^2 = 62.3\%$ ). C, Brain mapping of the corresponding brain pattern of the schizophrenia neurocognition signature. Positive weighting of voxels in red and negative weighting in blue color scale. D, Correlation of individual brain and cognition

scores derived from the applied schizophrenia neurocognition signature on patients with SCZ and healthy controls (HC) in C1 (dark blue,  $n = 131$ ;  $r = 0.49$ ;  $P < .001$ ,  $t$  test) and validation cohort C2 (orange,  $n = 160$ ;  $r = 0.31$ ;  $P < .001$ ,  $t$  test) with linear regression lines. E, Group-level comparison of individual cognition (left) and brain scores (right) from the schizophrenia neurocognition signature between HC ( $n_{C1} = 73$ ;  $n_{C2} = 84$ ) and SCZ ( $n_{C1} = 58$ ;  $n_{C2} = 76$ ) individuals in C1 (dark blue) and C2 (orange) cohorts using the Wilcoxon sum rank test (C1:  $P$  value<sub>brainscore</sub> =  $6.8e-07$ ;  $P$  value<sub>cognitionscore</sub> =  $1.15e-18$ ; C2:  $P$  value<sub>brainscore</sub> =  $8.7e-06$ ;  $P$  value<sub>cognitionscore</sub> =  $1.11e-22$ ). MRI indicates magnetic resonance imaging; NGN2, Neurogenin-2; rDLPFC, right dorsolateral prefrontal cortex.

<sup>a</sup>Indicates  $P < .001$ .

Based on the recently released CASTom-iGEx approach<sup>27</sup> combined with support vector regression (SVR), we predicted gene expression levels in iNs from genotype in cis and in trans (eMethods in Supplement 1).

### Reverse Personalized Dynamic Causal Modeling

We adapted a previously established canonical microcircuit Dynamic Causal Modeling (DCM) model<sup>28</sup> to develop a reverse personalized DCM (rpDCM) to link patient-specific in vitro synaptic density data with in vivo rsEEG signatures. Canonical microcircuit parameters were customized using empirically measured synapse data from iNs to simulate rsEEG-PSD via rpDCM. Implementation details, parameter mapping, and validation procedures are described in the eMethods in Supplement 1.

### Statistical Analysis

Multilayered associations between clinical and cognitive phenotype and GMV were identified using the sparse partial least-squares (SPLS) toolbox by Popovic and colleagues.<sup>29-31</sup> SPLS uses singular-value decomposition to extract latent variables (= multivariate signatures) that capture the shared covariance between 2 matrices—in our case, the cognitive phenotype matrix and the GMV matrix. By projecting each individual's data onto the weight vectors of the latent variable (eg, schizophrenia neurocognition signature), individualized latent scores (eg, cognition score and brain score) can be derived, providing individual loadings of these biobehavioral signatures that can be used for further downstream analyses (eMethods in Supplement 1).

Associations between the transcriptomic signatures, individualized cognition scores, brain score, and electrophysiological phenotypes were assessed using linear SVR models within the NeuroMiner platform.<sup>32,33</sup> Group comparisons and association analyses were performed using linear (mixed) or logistic regression models as indicated in the respective sections. Multiple comparisons correction was done where appropriate using the false discovery rate (FDR) method (eMethods in Supplement 1).

All analyses were conducted using MATLAB R2022a (MathWorks) and R (R Foundation); specifically, functions from the MATLAB Statistics and Machine Learning Toolbox, as well as the machine learning platform NeuroMiner, release version 1.3, were used. Two-tailed  $P < .05$  was considered significant.

## Results

### Structural Brain Alterations Linked to Cognitive Impairment in SCZ

To determine the behavioral consequences of changes in region-specific synaptic density, we considered alterations in GMV as approximate measure.<sup>1,10,11</sup> Based on previous evidence indicating structural brain alterations in SCZ,<sup>2,6,34</sup> we hypothesized that region-specific changes in GMV might particularly contribute to cognitive impairment as one critical clinical phenotype. To test this hypothesis, we sought to identify a multimodal signature of cognitive alterations in SCZ and its link to region-specific structural GMV brain changes in 2

deeply phenotyped cohorts (cohort 1 [C1]:  $n = 147$ ; mean [SD] age, 35.1 [11.6] years; 46 female participants [31.1%]; cohort 2 [C2]:  $n = 314$ ; mean [SD] age, 36.9 [11.7] years; 140 female participants [44.57%]) (Figure 1A; eTable 1 in Supplement 2). Within the discovery cohort (C1), the SPLS algorithm<sup>29</sup> identified 2 significant signatures, each representing a distinct combination of phenotypic (cognitive and clinical parameters) and structural GMV brain patterns.

In line with the literature,<sup>35,36</sup> the first aging signature represented a brain pattern of widespread GMV reduction (Spearman  $\rho = 0.78$ ;  $P < .001$ ;  $n = 131$ ) (eFigure 1A in Supplement 1; eTables 2-5 in Supplement 2).

The second schizophrenia neurocognition signature (Spearman  $\rho = 0.57$ ;  $P < .001$ ;  $n = 131$ ), which was independent of the age effect already captured by the aging signature, identified individuals with SCZ (positive weight; negative weight for HC) encompassing pronounced cognitive impairments in information processing, verbal long-term memory, cognitive flexibility, and working memory (indicated by negative weighting), as well as a higher disease severity (negative weight for age, positive weight for CPZeq) (Figure 1B; eFigure 1B in Supplement 1). This neurocognitive pattern was linked to a brain pattern of mainly GMV reductions in the frontotemporal regions, as well as the right insula, right DLPFC (rDLPFC), amygdala, and hippocampus and mapped predominantly to the default, limbic, control, and salience networks (Figure 1C; eFigure 1C in Supplement 1; eTables 2-5 in Supplement 2). Importantly, this signature was independent of sex.

By projecting the participants' data of validation cohort C2 onto the SPLS signature that was trained independently in C1, we could reveal that the cognition and brain scores were also significantly correlated in C2. Thereby, we successfully confirmed the generalizability of the schizophrenia neurocognition signature (Figure 1D), despite different study protocols regarding the applied cognitive tasks, as well as the MRI scanners.

Importantly, the latent brain and cognition scores—the individual loadings onto the schizophrenia neurocognition signature—were significantly higher in SCZ (Figure 1E). Finally, higher cognition (dysfunction) scores and brain scores were both linked to lower occupational rates, and higher cognition scores were associated with lower Global Assessment of Functioning scores (eFigure 2 in Supplement 1).

In summary, the SPLS analysis identified a schizophrenia neurocognition signature that captures a reproducible profile of severe cognitive impairments linked to a pattern of GMV loss within macrocircuits critical for cognitive function.<sup>8,37,38</sup>

### Patient-Level Neuronal Transcriptomes Associate With Brain Intermediate Phenotypes

Significant correlation of both scores with SCZ-PRS<sup>4</sup> indicated that the schizophrenia neurocognition signature captures trait-specific aspects of the illness within our cohorts of European ancestry (eFigure 3, eFigure 4A in Supplement 1). Of note, the cognition score showed a stronger association with SCZ-PRS than the brain score, suggesting that the clinical neurocognitive pattern of the schizophrenia neurocognition signature is closer associated to the trait-driven variability compared to its brain pattern.

Based on these findings and our previous iPSC study that identified molecular mechanisms of synapse dysfunction in SCZ,<sup>18</sup> we hypothesized that genetically driven alterations in neuron-related gene expression patterns contribute to the emergence of this signature. We therefore used the established iPSC cohort<sup>18</sup> (n = 80) of patients with SCZ and HCs that overlap with a subset of the translational cohorts C1 and C2 (Figure 1A).<sup>20</sup> Previously, we described the cohort-level in vitro differentiation into iNs (eFigure 4B in Supplement 1), giving rise to a deeply phenotyped personalized disease model library, including whole transcriptome profiles.<sup>18</sup> iN differentiation was performed in replicated batches across 2 centers to account for technical variability.<sup>18</sup> Importantly, extensive quality control of the iPSCs and the differentiated iNs showed no difference between case-control cell culture conditions, maturation state, or the general health of the iN cultures (eFigure 4C, eMethods in Supplement 1; see also our companion study<sup>18</sup>).

First, we leveraged the concept of transcriptome imputation,<sup>39</sup> predicting the gene expression pattern in iNs from the individual-level genotype using machine learning<sup>27</sup> in both clinical cohorts (eFigure 4D and E in Supplement 1). Importantly, differential expressed gene (DEG) patterns between SCZ and HC in iNs between predicted and the 310 empirical measured DEGs ( $\Delta$ SCZ-HC) were correlated ( $r = 0.45$ ;  $P$  value  $< 2.2e-16$ ,  $F$  test) with 75% of nominally significant genes exhibiting concordant direction of effect (eFigure 4F-H in Supplement 1; eTable 6 in Supplement 2).

Next, we explored whether the molecular variability in iN DEGs relates to the macro-scale intermediate phenotypes of the schizophrenia cognition signature (eFigure 5A in Supplement 1). We predicted the individual brain and cognition scores with the imputed DEG profiles of patients with SCZ and HC in C1 using SVR models in a repeated nested cross-validation pipeline, excluding individuals with empirically measured transcriptome profiles. This approach revealed a predictive capacity of the imputed iN DEGs to predict the individual cognition ( $r = 0.76$ ; 95% CI, 0.66-0.83;  $P < .001$ ; area under the curve [AUC] = 0.91) and brain scores ( $r = 0.39$ ; 95% CI, 0.21-0.55;  $P < .001$ ; AUC = 0.69) in the discovery cohort C1 (dark blue in Figure 2A; eFigure 5B in Supplement 1; eTables 7-9 in Supplement 2).<sup>40-44</sup>

Application of the trained SVR model to a held-out patient sample with empirically measured DEGs rather than imputed transcriptome profiles confirmed the predictive performance (light blue in Figure 2A; eFigure 5B in Supplement 1; cognition score:  $r = 0.77$ ; 95% CI, 0.57-0.89;  $P < .001$ ; AUC = 0.95; brain score:  $r = 0.31$ ; 95% CI, -0.07 to 0.60;  $P = .049$ ; AUC = 0.60). Similarly, replication analyses in the validation cohort C2 confirmed the generalizability of the iNs transcriptome-based prediction of the cognition ( $r = 0.17$ ; 95% CI, 0.028-0.31;  $P = .02$ ; AUC = 0.63) and the brain score ( $r = 0.23$ ; 95% CI, 0.07-0.37;  $P = .003$ ; AUC = 0.59), respectively (orange in Figure 2A; eFigure 5B in Supplement 1). Notably, these results were specific to the empirically determined iN DEG feature set, as both the imputed and the empirical DEG iN datasets significantly outperformed 100 models trained on randomized sets of iN genes and our previ-

ously published model<sup>27</sup> using imputed (postmortem) DLPFC gene expression (eFigure 5C in Supplement 1; eTables 10 and 11 in Supplement 2).

Interestingly, the iN DEGs were significantly enriched for synapse-related biological processes, and MAGMA gene-based analyses revealed direct associations with the SCZ GWAS for a substantial part (Figure 2B-C; eTables 12 and 13 in Supplement 2). Moreover, annotation-based analysis of the predictive gene features revealed the contribution of a substantial fraction of the 310 DEGs ( $\Delta$ SCZ-HC) to the prediction of the individual cognition and brain score (eFigure 5D in Supplement 1) including several neurotransmission-related genes, such as the calcium voltage-gated channel subunit alpha1A (*CACNA1A*) or the postsynaptic protein dishevelled binding antagonist of beta catenin 1 (*DACT1*) previously associated with neuronal and cognitive function.<sup>45,46</sup>

Jointly, these findings demonstrate that the variability of imputed and empirical measured molecular features from personalized iPSC-based disease models can partially explain the variability of SCZ-related phenotypes. Moreover, they implicate alterations in synaptic gene expression as an important contributor to cognitive impairment. Jointly, these findings support the hypothesis that regional GMV reductions arise in part from synaptic alterations.<sup>2</sup>

### Neurophysiological Consequences of Altered Brain Structure

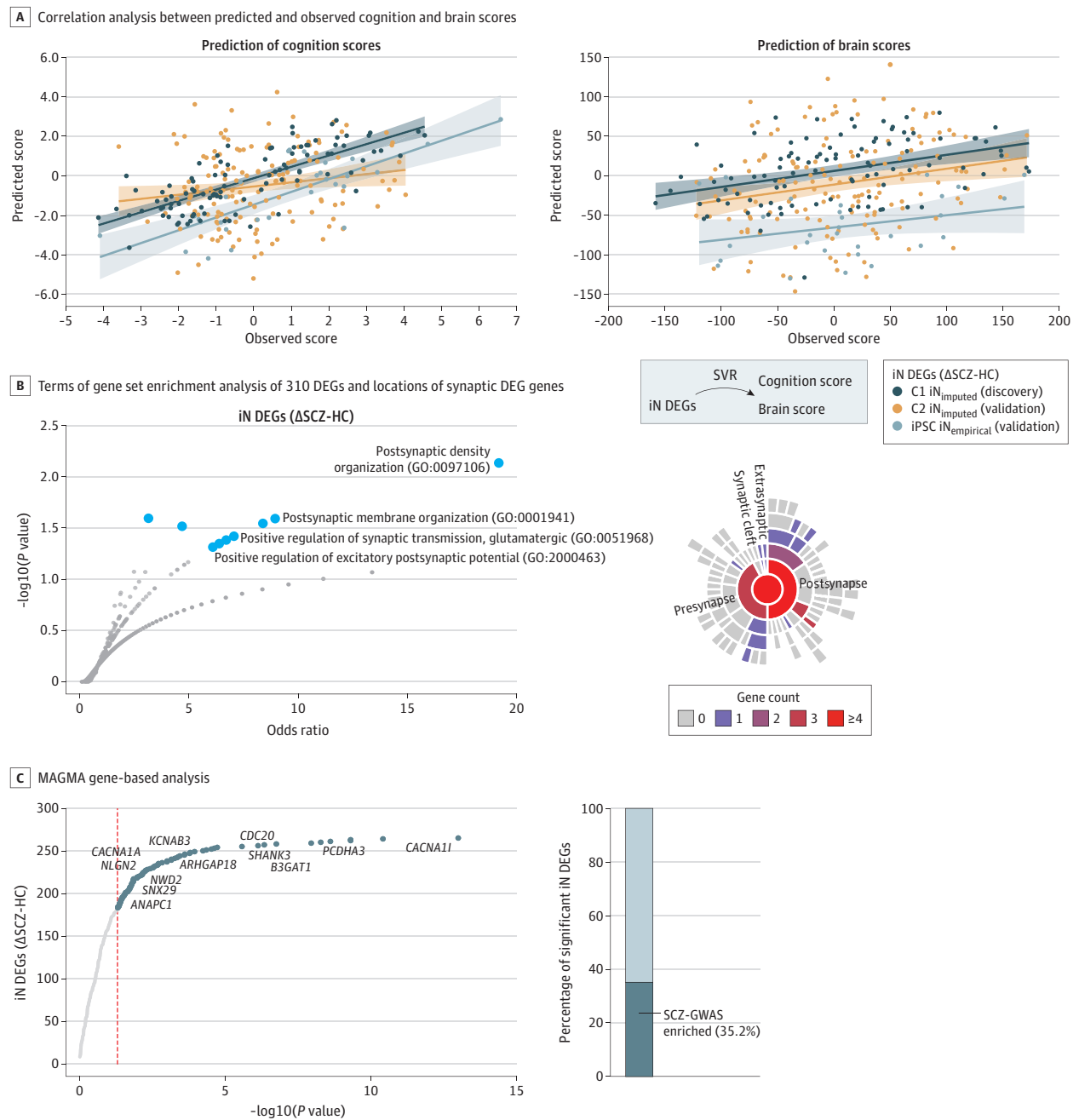
To test the hypothesis that changes in neuronal activity accompany alterations in GMV, we evaluated the link between the schizophrenia neurocognition signature and the brain's electrophysiological rsEEG (eyes closed) activity pattern, reflecting the aggregated postsynaptic potential.<sup>47</sup> In line with previous findings,<sup>48</sup> rsEEG-PSD analysis of available rsEEGs across C1 and C2 revealed an increase in theta and a decrease in gamma1 and gamma2 power in patients with SCZ (Figure 3A-B; eTable 14 in Supplement 2).

SVR-based prediction of the individual brain and cognition scores of the schizophrenia neurocognition signature from the matching patients' rsEEG-PSD revealed an association between neurophysiology and brain structure ( $r = 0.17$ ;  $P = .01$ ) and cognition ( $r = 0.2$ ;  $P = .004$ ) (Figure 3C). Interestingly, this link was largely driven by the variation in the theta and gamma range. Spatially, these changes were localized to the neighbored electrodes F8, F4, and T4, with F8 being the most predictive feature (Figure 3D; eTables 15-20 in Supplement 2) capturing rDLPFC brain activity, which is strongly involved in executive function and working memory.<sup>49</sup>

These findings on the electrophysiological level are consistent with the strong regional loadings of the schizophrenia neurocognition signature in the rDLPFC, which shows prominent GMV reductions that correlate with cognitive impairment (eFigure 6 in Supplement 1).

To further connect the macro-scale electrophysiological changes to their prospective molecular basis, we performed SVR-based prediction of SCZ-associated rsEEG-PSD (theta, gamma1, and gamma2) using iN DEG ( $\Delta$ SCZ-HC) imputed transcriptomic data. This analysis uncovered a significant association of the genetically determined imputed gene expression patterns

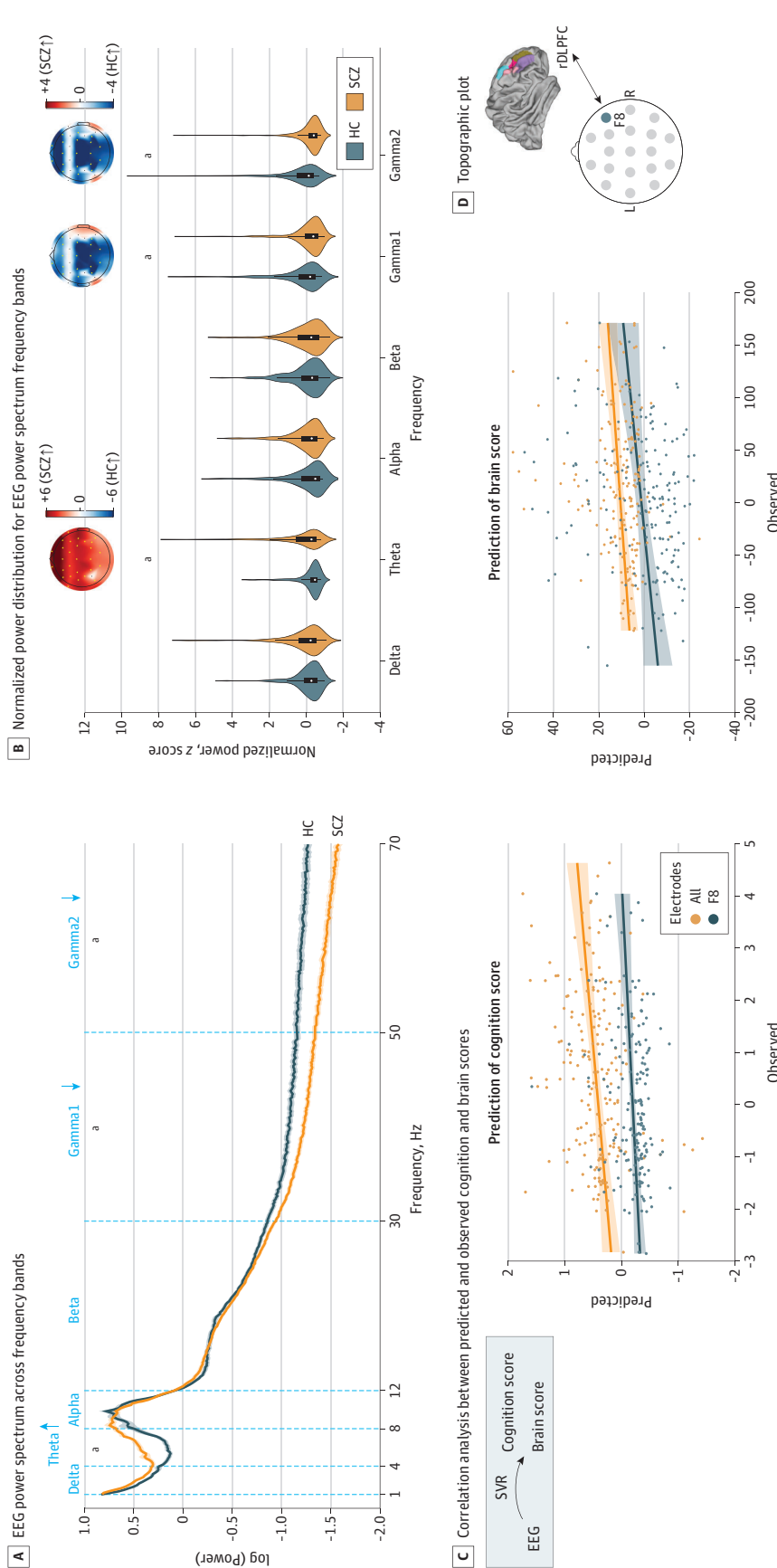
**Figure 2. Human Induced Pluripotent Stem Cell (iPSC)-Based Neuronal Transcriptome Predicts Individual Cognition and Brain Scores**



A, Correlation analysis between the predicted (y-axis) and observed (x-axis) cognition (left) and brain scores (right) of the schizophrenia neurocognition signature based on support vector regression (SVR) using imputed gene expression levels of 310 differential expressed genes (DEGs) ( $\Delta$ SCZ-HC) in iNs in discovery cohort 1 (C1  $iN_{imputed}$ , dark blue) and separate validation cohort 2 (C2  $iN_{imputed}$ , orange) and held-out empirically measured (not imputed) iN transcriptome data of the iPSC cohort ( $iPSC\ iN_{empirical}$ , light blue, deviating offset for visibility). Lines indicate linear regression model for all 3 cohorts for the cognition ( $n_{C1} = 98$ ;  $r_{C1} = 0.76$ ;  $p_{C1} = 0.0002$ ;  $n_{C2} = 153$ ;  $r_{C2} = 0.17$ ;  $p_{C2} = 0.016$ ;  $N_{iN} = 29$ ;  $r_{iN} = 0.77$ ;  $p_{iN} = 0.0002$ , permutation test) and brain scores ( $n_{C1} = 98$ ;  $r_{C1} = 0.39$ ;  $p_{C1} = 0.0002$ ;  $n_{C2} = 153$ ;  $r_{C2} = 0.23$ ;  $p_{C2} = 0.0026$ ;

$n_{iN} = 29$ ;  $r_{iN} = 0.31$ ;  $p_{iN} = 0.049$ , permutation test). B, Left: gene set enrichment analysis of the 310 DEGs ( $\Delta$ SCZ-HC) in iNs (eFigure 4 in Supplement 1; background gene set: iN transcriptome) using Enrichr.<sup>40-43</sup> Points represent gene sets with annotations for selected Gene ontology (GO) terms. Larger blue points denote significant GO terms ( $P < .05$ , not FDR corrected). Right: sunburst plot illustrating locations of synaptic DEG genes based on Synaptic Gene Ontologies.<sup>44</sup> C, Significance of gene-based association from MAGMA analysis of SCZ genome-wide association study (GWAS) summary statistics<sup>4</sup> plotted against the ranked list of iN DEGs (SCZ-HC). Significant genes are visualized in blue, selected genes are annotated. Bar plot visualizing percentage of iN DEGs significantly associated with SCZ GWAS<sup>4</sup> (dark blue).

**Figure 3. Electroencephalography (EEG) Power Spectrum Alterations in Schizophrenia (SCZ) Relate to Brain Structural and Neurocognitive Changes**

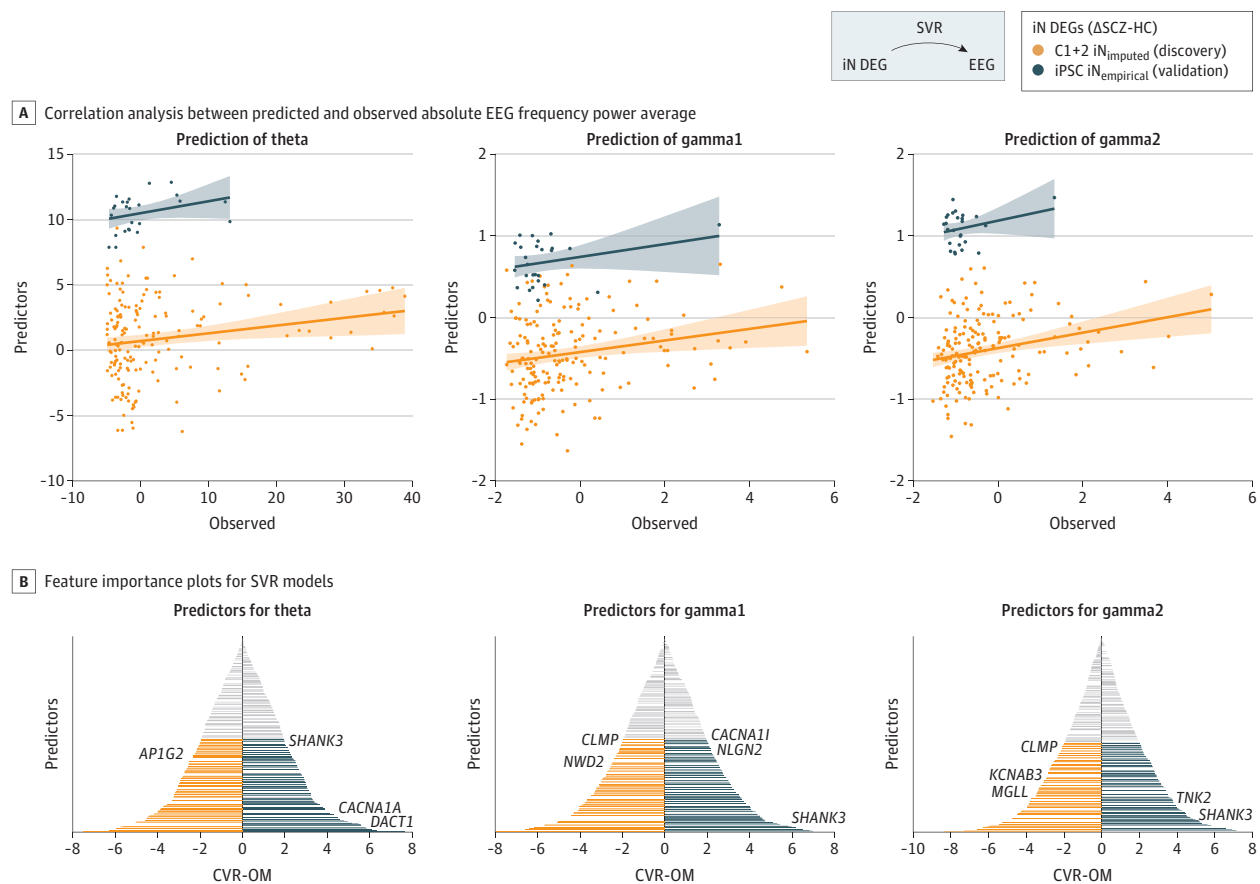


A. Resting-state EEG power spectrum (1-70 Hz, eyes closed) from 139 healthy controls (HC, blue line) and 217 patients with SCZ (orange line) across analyzed frequency bands delta, theta, alpha, beta, gamma1, and gamma2. Arrows and footnote indicate significant differences in SCZ compared to HC by Mann-Whitney *U* test (*P*[false discovery rate (FDR)] < .001;  $U_{\text{delta}} = 1.43621$ ,  $U_{\text{theta}} = 1.98$ ,  $U_{\text{alpha}} = 4.12$ ,  $U_{\text{beta}} = 0.09$ ,  $U_{\text{gamma1}} = -3.89$ ,  $U_{\text{gamma2}} = -5.97$ ). B. Violin plots depicting the normalized power (z scores) distribution for each resting-state EEG power spectrum frequency band in 139 HCs (blue) and 217 patients with SCZ (orange). Group comparison evaluated with Mann-Whitney *U* test ( $U_{\text{delta}} = 1.43621$ ,  $U_{\text{theta}} = 1.98$ ,  $U_{\text{alpha}} = 4.12$ ,  $U_{\text{beta}} = 0.09$ ,  $U_{\text{gamma1}} = -3.89$ ,  $U_{\text{gamma2}} = -5.97$ ). Topoplots illustrate alterations of the spatial EEG power distribution across the scalp in SCZ (heightened in red and diminished in blue). C. Correlation analysis between the predicted (y-axis) and observed (x-axis) cognition and brain scores of the schizophrenia neurocognition signature based on a nested cross-validated support vector regression (SVR) predicting the latter scores from individual EEG frequency band

power level in the theta, gamma1, and gamma2 frequency range across all electrodes in the joint C1 and C2 cohorts (orange). Predicted values result from predictions where the respective individual was held out in the outer fold of the nested cross-validation. Lines indicate linear regression between predicted and observed cognition ( $n = 191$ ;  $r = 0.2$ ;  $P < .001$ , permutation test) and brain score ( $n = 191$ ;  $r = 0.17$ ;  $P = .02$ , permutation test). In addition, SVR-based predictions only for the F8 electrode (blue) are shown (cognition score:  $n = 191$ ;  $r = 0.36$ ;  $P < .001$ , permutation test; brain score:  $n = 191$ ;  $r = 0.28$ ;  $P < .001$ , permutation test). D. Topo plot indicates the anatomical location of the F8 electrode as the top-ranking predictive feature with highest sum of cross-validation ratio overall mean in the cognition and brain score SVR analysis that reflects electrophysiological activity of the right dorsolateral prefrontal cortex (rDLPFC).

<sup>a</sup>Significant differences in SCZ compared to HC by Mann-Whitney *U* test ( $P$ [FDR] < .001).

Figure 4. Alterations in Synapse-Related Gene Expression Are Linked to Electroencephalography (EEG) Power Spectrum Alterations



A, Correlation analysis between the individual predicted (y-axis) and observed (x-axis) absolute EEG frequency power average over all electrodes in the theta (left), gamma1 (middle), and gamma2 (right) band. Prediction of the band power was performed using support vector regression (SVR) from genotype imputed gene expression levels of 310 induced pluripotent stem cell (iPSC)-derived excitatory pyramidal neuron (iN) differential expressed gene (DEGs) (Schizophrenia-healthy controls [ $\Delta$ SCZ-HC]) in a fused subset of individuals from cohort 1 (C1) and cohort 2 (C2) with available EEG data (C1 + 2 iN DEG<sub>imputed</sub>; n = 178; discovery, orange). Replication sample from a subset of held-out individuals of the iPSC cohort with empirically measured iN DEGs (iPSC iN DEG<sub>empirical</sub>; n = 26; validation, blue). The SVR model was trained using 5-fold cross-validation, and all predicted values are based on the held-out sample subsets. Lines indicate linear regression models between the observed

and predicted values for the discovery cohort and replication sample of theta ( $r_D = 0.185$ ;  $p_D$ [permutation test] = 0.006;  $r_{iN} = 0.26$ ;  $p_{iN}$ [permutation test] = 0.1), gamma1 ( $r_D = 0.174$ ;  $p_D$ [permutation test] = 0.01;  $r_{iN} = 0.28$ ;  $p_{iN}$ [permutation test] = 0.0788;  $p_{iN}$ [mean average error] = 0.0346), and gamma2 average band power ( $r_D = 0.22$ ;  $p_D$ [permutation test] = 0.001;  $r_{iN} = 0.28$ ;  $p_{iN}$ [permutation test] = 0.08;  $p_{iN}$ [mean average error] = 0.001), showing the replication iPSC sample with a different offset for better visibility. B, Feature importance plots for the SVR models depicting the ranked cross-validation ratio overall means ([CVR-OM], x-axis) of all gene features (y-axis) in the SVR model to predict the frequency band power for theta (left), gamma1 (middle), and gamma2 (right). Significant features are colored, with annotations for selected genes of interest.

in iNs with individual theta, gamma1, and gamma2 rsEEG-PSD variability (Figure 4A, in orange; range of theta, gamma1, and gamma2 predictions:  $r_D = 0.17$ -0.22;  $P$  values range, <.001-.01, permutation test; for details see Figure legend; eTables 21-26 in Supplement 2). Application of these models onto the empirically measured iN transcriptomes within the iPSC cohort replicated the prediction of the individual gamma1 and gamma2 rsEEG-PSD (Figure 4A, blue). Moreover, the link between DEG variability and gamma1 EEG band power was also evident at the level of the F8 electrode, which reflects rDLPFC's neuronal activity (eFigure 7 in Supplement 1). Importantly, a substantial part of the imputed iN DEGs ( $\Delta$ SCZ-HC) were predictive of the individual rsEEG-PSD variability, including several key synaptic genes, such as *SHANK3* or *NLGN2* (Figure 4B).

Jointly, these analyses link interindividual variability in molecular processes, contributing to synaptic function and brain structure,<sup>1,10,11</sup> to changes in patient-level electrophysiology.

#### Individual Synaptic Density Associates With Patients' Electrophysiology

However, despite the consistent link of neuroimaging-based regional structural brain changes with a reduction of synaptic density,<sup>1,10,11</sup> there remains a mechanistic gap between changes in gene expression levels, potential cellular consequences, and corresponding differences in patient-level intermediate and clinical phenotypes. We hypothesized that variability in synaptic density of patient-derived in vitro neuronal

networks constitute a suitable cellular endophenotype linked to individual differences in circuit-level electrophysiology. To test this hypothesis, we modified the DCM approach by Adams and colleagues<sup>28</sup> who studied different synaptic density parameters in silico to reproduce patient-level EEG power spectrum in a cohort that was independent from our study.<sup>28</sup> In this rpDCM, we used iPSC-derived neuronal networks to provide empirical assessments of individual synaptic density in vitro to predict the individual rsEEG-PSD levels in vivo (Figure 5A). We analyzed the frequency of the presynaptic bouton marker Synapsin 1 (SYN1) (Figure 5B; eFigure 8A in Supplement 1) of electrophysiologically active iN-derived neuronal networks<sup>18</sup> as an approximate measure for the density of functional synapses. To this end, SYN1 density within iN neurites was quantified by immunohistochemistry across 42 individuals (21 SCZ, 21 HC). This analysis revealed no differences in cell culture conditions (eFigure 8B and C in Supplement 1) but a significant mean reduction of excitatory synapses by 12.4% in SCZ that was independent of clinical (co)variables of their donors (Figure 5C; eTables 27 and 28 in Supplement 2). We then used the iN-synapse density to simulate the individual-level rsEEG-PSD of the same individual, setting all excitatory synaptic weights in the rpDCM to the empirically observed relative density (Figure 5D; eFigure 8D in Supplement 1). To test model specificity, we varied rpDCM parameters and found that only modulation of all or excitatory synapses were consistent with the EEG findings, but not inhibitory-only or subsets of excitatory synaptic connections (eFigure 9 in Supplement 1).

This rpDCM-simulated rsEEG power spectrum qualitatively recapitulated the groupwise differences of the empirical rsEEG, including the significant differences in the theta and gamma frequency range (Figure 5E; eFigure 10 in Supplement 1). Beyond groupwise differences, we detected nominally ( $P \leq .05$ ) significant correlations between the individual level of simulated and empirical rsEEG-PSD in the gamma range at the C3, C4, and F8 electrodes (Figure 5F; eTables 29 and 30 in Supplement 2), of which the latter passed multiple testing correction ( $q$  value = 0.017), providing an intrapersonal biophysical link between variability in synaptic density and changes in the rDLPFC's gamma1 rsEEG-PSD.

## Discussion

This study bridges the translational gap in SCZ by linking synaptic deficits of excitatory neurons to individual changes in brain structure, electrophysiology, and cognitive impairments. Our schizophrenia neurocognition signature identified a pattern of GMV reduction, likely reflecting loss of synapses and dendritic complexity,<sup>1,10,11</sup> with a pronounced contribution of the rDLPFC. This brain pattern is associated with cognitive impairments and linked to electrophysiological alterations, particularly in the gamma frequency range.

While iPSC modeling is powerful, it remains a time- and cost-intensive bottleneck.<sup>50</sup> To scale multimodal integration in our deep phenotyped cohorts, we imputed gene expression profiles in silico using genotype data.<sup>27</sup> We used excitatory iN, which showed substantial gene expression altera-

tions and reduced synapse density in SCZ, to enable the intraindividual translation of genetically driven individual cell-autonomous variability into the individual degree of brain circuitry, electrophysiology, and cognitive changes.

By the reverse adaption of the DCM from Adams and colleagues,<sup>28</sup> established and trained independently from our cohorts, our rpDCM approach showed that synaptic deficits of excitatory neurons were associated with altered neurophysiology in SCZ. The finding that gamma1-PSD at the F8 electrode—reflecting rDLPFC activity—showed the strongest association with synapse density aligns with the converging evidence across our multimodal study: rDLPFC was prominently involved in the SPLS-derived schizophrenia neurocognition signature and drove EEG-brain score associations. This aligns with the established roles of the rDLPFC<sup>49</sup> and lower gamma band power<sup>48</sup> in cognitive impairments in SCZ.

Importantly, our results are in line with the hypothesis that a reduction in excitatory synaptic function progressively contributes to localized cortical disinhibition.<sup>1</sup> Comparing alternative configurations of our rpDCM revealed that only the modulation of all synapses or the excitatory synapses alone reproduced the rsEEG-PSD group differences, while an inhibitory-only modulation failed to do so, supporting the contribution of excitatory neurons to the observed changes in EEG power. Thus, by linking patient-specific molecular and synaptic deficits of excitatory neurons to intermediate phenotypes of SCZ, our multilayer modeling supports both the long-standing glutamate hypothesis—postulating disrupted excitatory neurotransmission—and Feinberg's synaptic hypothesis.<sup>1,51</sup>

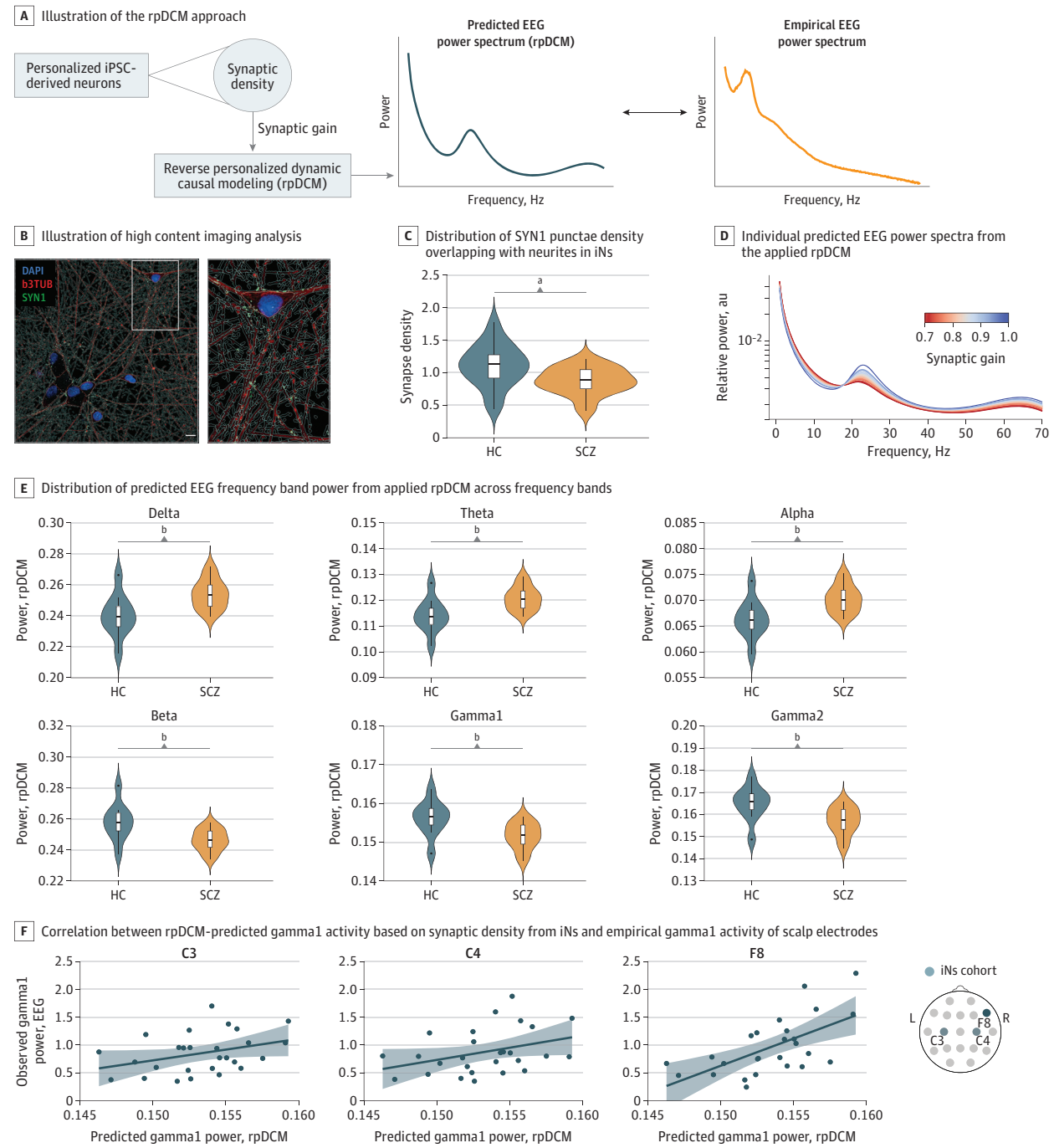
## Limitations

Despite encouraging findings, several limitations remain. First, modeling was limited to excitatory neurons. Future refinements should incorporate diverse cell types implicated in SCZ,<sup>52-55</sup> including fast-spiking GABAergic interneurons—critical for gamma oscillations<sup>48,56</sup>—and glial cells to enrich translational disease modeling. Moreover, the extension of translational phenotype batteries that can be assessed in vivo and in vitro, such as connectivity measurements (eg, task and resting-state functional MRI and multielectrode arrays) or measurement of neurotransmitter concentrations (eg, magnetic resonance spectroscopy, metabolomics), will be an essential prerequisite to further advance this intraindividual translational approach.

Second, while maturation states of iN from the investigated iPSC donors were comparable, future longitudinal studies will be needed to determine whether the identified molecular and synaptic deficits arise during early development or later maturation.

Third, iPSC models do not account for environmental contributions to SCZ, such as perinatal infections, nutritional deficits, substance use, trauma, and stress,<sup>57</sup> which may interact with genetic predisposition to shape brain structure and function. Our results suggest that synaptic pathology contributes upstream to these macro-scale changes, but a more complete understanding requires integration of environmental variables.

**Figure 5. Reverse Personalized Dynamic Causal Modeling (rpDCM) Predicts Individual Electroencephalography (EEG) Gamma Power Based on Intraindividual Synaptic Density From Induced Pluripotent Stem Cell (iPSC)-Derived Excitatory Pyramidal Neurons (iN)**



A, Illustration of the rpDCM approach, adapted from Adams et al.<sup>28</sup> integrating measured excitatory synaptic density iNs as a proxy for synaptic gain to predict EEG power spectra. B, Imaging analysis with neurite segmentation masks based on immunocytochemistry with Synapsin 1 (SYN1, green),  $\beta$ 3-tubulin ( $\beta$ 3TUB, red), and DAPI nuclei staining (blue). Scale bar = 10  $\mu$ m. C, SYN1 density in iNs from HC (n = 21) and SCZ (n = 21); total of 107 wells/coverslips from  $\geq 2$  independent differentiation batches). D, Predicted EEG power spectra from the applied rpDCM of the translational iPSC cohort (n = 42). E, Distribution of

frequency bands in the rpDCM-predicted EEG power spectrum in HC (n = 10) and SCZ (n = 20). F, Intraindividual correlation between rpDCM-predicted gamma1 activity and empirical EEG gamma1 activity of the scalp electrodes C3 ( $r = 0.45$ ;  $P = .048$ ; n = 27), C4 ( $r = 0.43$ ;  $P = .05$ ; n = 27), and F8 ( $r = 0.63$ ;  $P < .001$ ; n = 26). Gray areas = confidence intervals. Illustration of the highlighted electrodes. <sup>a</sup>SCZ-HC group differences ( $P = .02$ ; 2-tailed linear mixed model). <sup>b</sup>SCZ-HC group differences ( $P < .01$ ; 2-tailed linear mixed model).

Fourth, despite the power of our genetic imputation approach, its generalizability remains poor and larger iN cohorts are required to improve the explanatory capacity and generalizability of this strategy. Thus, the establishment of substantially larger translational deep phenotype cohorts with matching iPSCs ( $N > 200$ ) will be instrumental to obtain sufficient detection power and mitigate the high level of clinical heterogeneity in SCZ. Furthermore, the generalizability of our developed models is still limited, which might be due to different phenotyping protocols between the cohorts, different MRI scanners, and experimental variability at the level of iPSC cultivation and differentiation.

## Conclusions

In summary, our findings in this genetic association study support an integrated model in which genetic predisposition, act-

ing through altered expression of synaptic genes, leads to reduced excitatory synaptic density in key cortical and subcortical regions. These cellular-level changes of synapse density, potentially amplified by environmental factors, then contribute to widespread structural and functional brain alterations, including reduced gamma band power, and thereby contribute to cognitive impairment in SCZ.

This proof-of-concept study establishes a generally applicable strategy to bridge the gap between cellular endophenotypes, modeled in vitro, and in vivo clinical intermediate phenotypes. Linking iPSC-derived cellular data with clinical imaging, EEG, and cognitive profiles by the use of machine learning strategies and rpDCM, we outline a strategy for future biomarker discovery and precision psychiatry. Ultimately, multilayered translational frameworks could accelerate development of targeted, mechanism-based treatments for cognitive dysfunction in SCZ.

### ARTICLE INFORMATION

**Accepted for Publication:** February 9, 2026.

**Published Online:** March 28, 2026.  
doi:10.1001/jamapsychiatry.2026.0576

**Open Access:** This is an open access article distributed under the terms of the [CC-BY License](#).  
© 2026 Raabe FJ et al. *JAMA Psychiatry*.

**Author Affiliations:** Max Planck Institute of Psychiatry, Munich, Germany (Raabe, Popovic, Fischer, Boudriot, Jiang, Roell, Schmitt, Koutsouleris, Papiol, Falkai, Ziller); Department of Psychiatry and Psychotherapy, University Hospital, Ludwig-Maximilians-Universität (LMU) Munich, Munich, Germany (Raabe, Popovic, Vetter, Hasanaj, Karšli, Boudriot, Yakimov, Weyer, Roell, Moussiopoulou, Krčmář, Galinski, Pogarell, Schmitt, Koutsouleris, Rossner, Falkai, Keeser); Neuroimaging Core Unit Munich, University Hospital, LMU Munich, Munich, Germany (Hasanaj, Karšli, Roell, Keeser); Evidence-Based Psychiatry and Psychotherapy, Faculty of Medicine, University of Augsburg, Augsburg, Germany (Hasanaj, Wagner); University of Tübingen, Tübingen, Germany (Schäfer, Levina); Max Planck Institute for Biological Cybernetics, Tübingen, Germany (Schäfer, Levina); Department of Psychiatry, University of Münster, Münster, Germany (Almeida, Atella, Gagliardi, Trastulla, Ziller); Center for Soft Nanoscience, University of Münster, Münster, Germany (Almeida, Atella, Gagliardi, Trastulla, Ziller); International Max Planck Research School for Translational Psychiatry, Munich, Germany (Yakimov); Systasy Bioscience GmbH, Munich, Germany (Galinski, Rossner); Department of Psychiatry, Psychotherapy, and Psychosomatics, Medical Faculty, University of Augsburg, Augsburg, Germany (Papazova, Hasan, Wagner); German Center for Mental Health, partner site Munich-Augsburg, Munich, Germany (Hasan, Schulte, Schmitt, Koutsouleris, Falkai); Institute of Human Genetics, University Hospital, Faculty of Medicine, University of Bonn, Bonn, Germany (Schulte); Department of Psychiatry and Psychotherapy, University Hospital, Faculty of Medicine, University of Bonn, Bonn, Germany (Schulte); Institute of Psychiatric Phenomics and Genomics, University Hospital, LMU Munich, Munich, Germany (Schulte, Papiol); Laboratory of Neurosciences, Institute of Psychiatry, University of

São Paulo, São Paulo, Brazil (Schmitt); Institute of Psychiatry, Psychology and Neuroscience, King's College London, London, United Kingdom (Koutsouleris); Munich Center for Neurosciences, LMU Munich, Planegg-Martinsried, Germany (Keeser).

**Author Contributions:** Drs Raabe and Ziller had full access to all of the data in the study and take responsibility for the integrity of the data and the accuracy of the data analysis. Drs Raabe and Popovic and Drs Keeser and Ziller are joint first and joint last authors, respectively.

**Concept and design:** Raabe, Moussiopoulou, Krčmář, Pogarell, Hasan, Schmitt, Koutsouleris, Levina, Wagner, Rossner, Keeser, Ziller.

**Acquisition, analysis, or interpretation of data:** Raabe, Popovic, Vetter, Fischer, Hasanaj, Karšli, Schäfer, Almeida, Atella, Gagliardi, Boudriot, Yakimov, Trastulla, Jiang, Weyer, Röll, Moussiopoulou, Galinski, Papazova, Pogarell, Schulte, Papiol, Falkai, Keeser, Ziller, CDP Working Group.

**Drafting of the manuscript:** Raabe, Popovic, Vetter, Gagliardi, Hasan, Schmitt, Wagner, Keeser, Ziller.

**Critical review of the manuscript for important intellectual content:** Popovic, Vetter, Fischer, Hasanaj, Karšli, Schäfer, Almeida, Atella, Boudriot, Yakimov, Trastulla, Jiang, Weyer, Röll, Moussiopoulou, Krčmář, Galinski, Papazova, Pogarell, Hasan, Schulte, Schmitt, Koutsouleris, Levina, Wagner, Rossner, Papiol, Falkai, Keeser, Ziller.

**Statistical analysis:** Raabe, Popovic, Vetter, Fischer, Hasanaj, Karšli, Schäfer, Boudriot, Trastulla, Jiang, Weyer, Röll, Hasan, Schulte, Koutsouleris, Papiol, Keeser, Ziller.

**Obtained funding:** Raabe, Hasan, Schulte, Schmitt, Levina, Rossner, Keeser, Ziller.

**Administrative, technical, or material support:** Raabe, Almeida, Yakimov, Moussiopoulou, Krčmář, Pogarell, Schmitt, Rossner, Keeser, Ziller.

**Supervision:** Raabe, Popovic, Moussiopoulou, Pogarell, Hasan, Schulte, Schmitt, Koutsouleris, Levina, Wagner, Rossner, Falkai, Keeser, Ziller.

**Conflict of Interest Disclosures:** Dr Popovic reported grants from the Else Kröner-Fresenius-Stiftung during the conduct of the study. Dr Schäfer reported grants from Deutsche Forschungsgemeinschaft (DFG),

German Research Foundation) and the Else Kröner-Fresenius-Stiftung during the conduct of the study. Dr Boudriot reported grants from the Pesl Alzheimer Foundation during the conduct of the study. Dr Galinski reported personal fees from Systasy Bioscience GmbH outside the submitted work. Dr Hasan reported personal fees from AbbVie, Axuno, Boehringer Ingelheim, Janssen, Lundbeck, Otsuka, Recordati, Rovi, and Teva outside the submitted work. Dr Schmitt reported grants from the Else Kröner-Fresenius-Stiftung and nonfinancial support from the German Center of Mental Health during the conduct of the study. Dr Wagner reported personal fees from Boehringer Ingelheim, Lundbeck, Recordati, and Teva outside the submitted work. Dr Papiol reported grants from the Horizon Europe research and innovation program (grant agreement 101057454) outside the submitted work. Dr Keeser reported support for the procurement of the magnetic resonance imaging scanner from the DFG grant for major research (DFG, INST 86/1739-1 FUGG) during the conduct of the study. Dr Ziller reported personal fees from Novartis AG outside the submitted work. No other disclosures were reported.

**Funding/Support:** This work was supported by the Federal Ministry of Education and Research (Bundesministerium für Bildung und Forschung [BMBF]), eMed grant numbers O1ZX1504, O1ZX1706A (Dr Ziller); the Else Kröner-Fresenius-Stiftung grant A54 (Dr Ziller); and Deutsche Forschungsgemeinschaft (DFG, German Research Foundation) grants GZ: ZI 1614/5-1, ZI 1614/7-1 (Dr Ziller). The procurement of the magnetic resonance imaging scanner was supported by the DFG grant for major research (DFG, INST 86/1739-1 FUGG). Dr Boudriot received funding from the Pesl-Alzheimer-Stiftung (2024-2025). Drs Raabe and Popovic were supported by the Else Kröner-Fresenius-Stiftung (Research College "Translational Psychiatry") for their residency/PhD track at the International Max Planck Research School for Translational Psychiatry (IMPRS-TP). Drs Raabe and Schulte were supported by the Munich Clinician Scientist Program of the Faculty of Medicine, Ludwig-Maximilians-Universität (LMU) Munich (FöFoLe 009/2019 and Advanced Track 01/2021, respectively). Dr Raabe received funding from the Lisa Oehler-Stiftung (2022-2024) and the

Pesl-Alzheimer-Stiftung (2024-2025). Dr Yakimov was supported by the residency/PhD track of the IMPRS-TP and was supported by the Faculty of Medicine at LMU Munich (FöFoLe Reg.-Nr. 1226/2024). Dr Moussiopoulou was supported by the Faculty of Medicine at LMU Munich (FöFoLe Reg.-Nr. 1167). The study was supported by the EU HORIZON-INFRA-2024-TECH-01-04 project DTRIP4H 101188432 to Drs Raabe, Schmitt, and Falkai. Drs Hasanaj, Yakimov, Schmitt, and Falkai received funding from the BMBF within the Era-Net Neuron project GDNF\_UpReg (FKZ 01EW2206). The study was endorsed by the Federal Ministry of Education and Research (BMBF) within the initial phase of the German Center for Mental Health (DZPG) (grant: 01EE2303C to Dr Hasan, and 01EE2303A, 01EE2303F to Dr Falkai). The study was supported by the Supplement to BMBF funding for DZPG by the Bavarian State Ministry for Science and the Arts with the grant for the research project "Improving Infrastructures for DZPG and NAKO Cohorts" to Drs Karshi, Falkai, and Keeser. Dr Schäfer received funding through the Else Kröner Medical Scientist Kolleg "ClinBrAln: Artificial Intelligence for Clinical Brain Research" and is supported by IMPRS-Intelligent Systems. Dr Levina is a member of the Machine Learning Cluster of Excellence, EXC number 2064/1, project number 39072764.

**Role of the Funder/Sponsor:** The funders had no role in the design and conduct of the study; collection, management, analysis, and interpretation of the data; preparation, review, or approval of the manuscript; and decision to submit the manuscript for publication.

**Group Information:** The CDP Working Group investigators and coordinators are listed in Supplement 3.

**Data Sharing Statement:** See Supplement 4.

**Additional Contributions:** We thank all patients for their participation making this study possible. We thank Rick Adams, PhD (Institute of Cognitive Neuroscience, University College London), for sharing the dynamic-causal modeling code and helpful discussions. Dr Adams was not compensated for his work.

**Additional Information:** The CDP Working Group is affiliated with the Max Planck Institute of Psychiatry; the Department of Psychiatry and Psychotherapy, University Hospital, Ludwig-Maximilians-Universität (LMU) Munich; the Neuroimaging Core Unit Munich, University Hospital, LMU Munich; the Department of Psychiatry, Psychotherapy, and Psychosomatics, Medical Faculty, University of Augsburg; Department of Psychiatry and Psychotherapy, University Hospital, Faculty of Medicine, University of Bonn; and Department of Psychiatry, University of Münster.

## REFERENCES

- Howes OD, Onwordi EC. The synaptic hypothesis of schizophrenia version III: a master mechanism. *Mol Psychiatry*. 2023;28(5):1843-1856. doi:10.1038/s41380-023-02043-w
- Howes OD, Cummings C, Chapman GE, Shatalina E. Neuroimaging in schizophrenia: an overview of findings and their implications for synaptic changes. *Neuropsychopharmacology*. 2023;48(1):151-167. doi:10.1038/s41386-022-01426-x

- Lam M, Hill WD, Trampush JW, et al. Pleiotropic meta-analysis of cognition, education, and schizophrenia differentiates roles of early neurodevelopmental and adult synaptic pathways. *Am J Hum Genet*. 2019;105(2):334-350. doi:10.1016/j.ajhg.2019.06.012
- Trubetskoy V, Pardiñas AF, Qi T, et al; Indonesia Schizophrenia Consortium; PsychENCODE; Psychosis Endophenotypes International Consortium; SynGO Consortium; Schizophrenia Working Group of the Psychiatric Genomics Consortium. Mapping genomic loci implicates genes and synaptic biology in schizophrenia. *Nature*. 2022;604(7906):502-508. doi:10.1038/s41586-022-04434-5
- Liloia D, Brasso C, Cauda F, et al. Updating and characterizing neuroanatomical markers in high-risk subjects, recently diagnosed and chronic patients with schizophrenia: a revised coordinate-based meta-analysis. *Neurosci Biobehav Rev*. 2021;123:83-103. doi:10.1016/j.neubiorev.2021.01.010
- Goodkind M, Eickhoff SB, Oathes DJ, et al. Identification of a common neurobiological substrate for mental illness. *JAMA Psychiatry*. 2015;72(4):305-315. doi:10.1001/jamapsychiatry.2014.2206
- Huang K, Kang Y, Wu Z, Wang Y, Cai S, Huang L. Asymmetrical alterations of grey matter among psychiatric disorders: a systematic analysis by voxel-based activation likelihood estimation. *Prog Neuropsychopharmacol Biol Psychiatry*. 2021;110:110322. doi:10.1016/j.pnpbp.2021.110322
- Picó-Pérez M, Vieira R, Fernández-Rodríguez M, De Barros MAP, Radua J, Morgado P. Multimodal meta-analysis of structural gray matter, neurocognitive and social cognitive fMRI findings in schizophrenia patients. *Psychol Med*. 2022;52(4):614-624. doi:10.1017/S0033291721005523
- van Erp TGM, Walton E, Hibar DP, et al; Karolinska Schizophrenia Project. Cortical brain abnormalities in 4474 individuals with schizophrenia and 5098 control subjects via the Enhancing Neuro Imaging Genetics Through Meta Analysis (ENIGMA) Consortium. *Biol Psychiatry*. 2018;84(9):644-654. doi:10.1016/j.biopsych.2018.04.023
- Kassem MS, Lagopoulos J, Stait-Gardner T, et al. Stress-induced grey matter loss determined by MRI is primarily due to loss of dendrites and their synapses. *Mol Neurobiol*. 2013;47(2):645-661. doi:10.1007/s12035-012-8365-7
- Keifer OP Jr, Hurt RC, Gutman DA, Keilholz SD, Gourley SL, Ressler KJ. Voxel-based morphometry predicts shifts in dendritic spine density and morphology with auditory fear conditioning. *Nat Commun*. 2015;6:7582. doi:10.1038/ncomms8582
- Fish KN, Sweet RA, MacDonald ML, Lewis DA. Regional specificity of cortical layer 3 dendritic spine deficits in schizophrenia. *JAMA Psychiatry*. 2025;82(11):1123-1132. doi:10.1001/jamapsychiatry.2025.2221
- Maran M, Grent 't-Jong T, Uhlhaas PJ. Electrophysiological insights into connectivity anomalies in schizophrenia: a systematic review. *Neuropsychiatr Electrophysiol*. 2016;2(1). doi:10.1186/s40810-016-0020-5
- Perrotelli A, Giordano GM, Brando F, et al. Unveiling the associations between EEG indices and cognitive deficits in schizophrenia-spectrum disorders: a systematic review. *Diagnostics (Basel)*. 2022;12(9):2193. doi:10.3390/diagnostics12092193
- Hong Y, Yang Q, Song H, Ming GL. Opportunities and limitations for studying neuropsychiatric disorders using patient-derived induced pluripotent stem cells. *Mol Psychiatry*. 2023;28(4):1430-1439. doi:10.1038/s41380-023-01990-8
- Räsänen N, Tiihonen J, Koskivi M, Lehtonen Š, Koistinaho J. The iPSC perspective on schizophrenia. *Trends Neurosci*. 2022;45(1):8-26. doi:10.1016/j.tins.2021.11.002
- Rowe RG, Daley GQ. Induced pluripotent stem cells in disease modelling and drug discovery. *Nat Rev Genet*. 2019;20(7):377-388. doi:10.1038/s41576-019-0100-z
- Raabe FJ, Hausrucking A, Gagliardi M, et al. Polygenic risk for schizophrenia converges on alternative polyadenylation as molecular mechanism underlying synaptic impairment. *bioRxiv*. 2024;doi:10.1101/2024.01.09.574815
- Mäki-Marttunen T, Kaufmann T, Elvsåshagen T, et al. Biophysical psychiatry-how computational neuroscience can help to understand the complex mechanisms of mental disorders. *Front Psychiatry*. 2019;10:534. doi:10.3389/fpsy.2019.00534
- Krčmář L, Jäger I, Boudriot E, et al. The multimodal Munich Clinical Deep Phenotyping Study to bridge the translational gap in severe mental illness treatment research. *Front Psychiatry*. 2023;14:1179811. doi:10.3389/fpsy.2023.1179811
- Berk M, Kim JH, Williams LJ, et al. A novel discovery platform for targeted drug repurposing: application for psychiatric disorders. *Lancet Psychiatry*. 2025;12(7):535-542. doi:10.1016/S2215-0366(25)00066-5
- Budde M, Anderson-Schmidt H, Gade K, et al. A longitudinal approach to biological psychiatric research: the PsyCourse study. *Am J Med Genet B Neuropsychiatr Genet*. 2019;180(2):89-102. doi:10.1002/ajmg.b.32639
- Keefe RSE, Goldberg TE, Harvey PD, Gold JM, Poe MP, Coughenour L. The Brief Assessment of Cognition in Schizophrenia: reliability, sensitivity, and comparison with a standard neurocognitive battery. *Schizophr Res*. 2004;68(2-3):283-297. doi:10.1016/j.schres.2003.09.011
- Leucht S, Samara M, Heres S, Davis JM. Dose equivalents for antipsychotic drugs: the DDD method. *Schizophr Bull*. 2016;42(Suppl 1)(suppl 1):S90-S94. doi:10.1093/schbul/sbv167
- Vallat R, Walker MP. An open-source, high-performance tool for automated sleep staging. *Elife*. 2021;10:e70092. doi:10.7554/eLife.70092
- Ge T, Chen CY, Ni Y, Feng YA, Smoller JW. Polygenic prediction via Bayesian regression and continuous shrinkage priors. *Nat Commun*. 2019;10(1):1776. doi:10.1038/s41467-019-09718-5
- Trastulla L, Dolgalev G, Moser S, et al; Schizophrenia Working Group of the Psychiatric Genomics Consortium. Distinct genetic liability profiles define clinically relevant patient strata across common diseases. *Nat Commun*. 2024;15(1):5534. doi:10.1038/s41467-024-49338-2
- Adams RA, Pinotsis D, Tsirlis K, et al. Computational modeling of electroencephalography and functional magnetic resonance imaging paradigms indicates a consistent loss of pyramidal cell synaptic gain in schizophrenia. *Biol Psychiatry*.

- 2022;91(2):202-215. doi:10.1016/j.biopsych.2021.07.024
29. Popovic D, Ruef A, Dwyer DB, et al; PRONIA Consortium. Traces of trauma: a multivariate pattern analysis of childhood trauma, brain structure, and clinical phenotypes. *Biol Psychiatry*. 2020;88(11):829-842. doi:10.1016/j.biopsych.2020.05.020
30. Monteiro JM, Rao A, Shawe-Taylor J, Mourão-Miranda J; Alzheimer's Disease Initiative. A multiple hold-out framework for sparse partial least squares. *J Neurosci Methods*. 2016;271:182-194. doi:10.1016/j.jneumeth.2016.06.011
31. SPLS\_Toolbox\_2022. GitHub. Accessed March 17, 2026. [https://github.com/molgen.mpg.de/DavidPopovic/SPLS\\_Toolbox\\_2022](https://github.com/molgen.mpg.de/DavidPopovic/SPLS_Toolbox_2022)
32. Dwyer DB, Falkai P, Koutsouleris N. Machine learning approaches for clinical psychology and psychiatry. *Annu Rev Clin Psychol*. 2018;14:91-118. doi:10.1146/annurev-clinpsy-032816-045037
33. NeuroMiner. GitHub. Accessed March 17, 2026. <https://github.com/neurominer-git/NeuroMiner>
34. Sha Z, Wager TD, Mechelli A, He Y. Common dysfunction of large-scale neurocognitive networks across psychiatric disorders. *Biol Psychiatry*. 2019;85(5):379-388. doi:10.1016/j.biopsych.2018.11.011
35. Fjell AM, Walhovd KB. Structural brain changes in aging: courses, causes and cognitive consequences. *Rev Neurosci*. 2010;21(3):187-221. doi:10.1515/REVNEURO.2010.21.3.187
36. Jernigan TL, Archibald SL, Fennema-Notestine C, et al. Effects of age on tissues and regions of the cerebrum and cerebellum. *Neurobiol Aging*. 2001;22(4):581-594. doi:10.1016/s0197-4580(01)00217-2
37. Karantonis JA, Carruthers SP, Rossell SL, et al. A systematic review of cognition-brain morphology relationships on the schizophrenia-bipolar disorder spectrum. *Schizophr Bull*. 2021;47(6):1557-1600. doi:10.1093/schbul/sbab054
38. Kraguljac NV, McDonald WM, Widge AS, Rodríguez CI, Tohen M, Nemeroff CB. Neuroimaging biomarkers in schizophrenia. *Am J Psychiatry*. 2021;178(6):509-521. doi:10.1176/appi.ajp.2020.20030340
39. Wainberg M, Sinnott-Armstrong N, Mancuso N, et al. Opportunities and challenges for transcriptome-wide association studies. *Nat Genet*. 2019;51(4):592-599. doi:10.1038/s41588-019-0385-z
40. Chen EY, Tan CM, Kou Y, et al. Enrichr: interactive and collaborative HTML5 gene list enrichment analysis tool. *BMC Bioinformatics*. 2013;14:128. doi:10.1186/1471-2105-14-128
41. Kuleshov MV, Jones MR, Rouillard AD, et al. Enrichr: a comprehensive gene set enrichment analysis web server 2016 update. *Nucleic Acids Res*. 2016;44(W1):W90-7. doi:10.1093/nar/gkw377
42. Aleksander SA, Balhoff J, Carbon S, et al; Gene Ontology Consortium. The Gene Ontology knowledgebase in 2023. *Genetics*. 2023;224(1):iyad031. doi:10.1093/genetics/iyad031
43. Clarke DJB, Jeon M, Stein DJ, et al. Apyters: turning Jupyter Notebooks into data-driven web apps. *Patterns (N Y)*. 2021;2(3):100213. doi:10.1016/j.patter.2021.100213
44. Koopmans F, van Nierop P, Andres-Alonso M, et al. SynGO: an evidence-based, expert-curated knowledge base for the synapse. *Neuron*. 2019;103(2):217-234.e4. doi:10.1016/j.neuron.2019.05.002
45. Okerlund ND, Kivimäe S, Tong CK, Peng IF, Ullian EM, Cheyette BN. Dact1 is a postsynaptic protein required for dendrite, spine, and excitatory synapse development in the mouse forebrain. *J Neurosci*. 2010;30(12):4362-4368. doi:10.1523/JNEUROSCI.0354-10.2010
46. Humbertclaude V, Riant F, Krams B, et al; Episodic Syndrome Consortium. Cognitive impairment in children with CACNA1A mutations. *Dev Med Child Neurol*. 2020;62(3):330-337. doi:10.1111/dmcn.14261
47. Kirschstein T, Köhling R. What is the source of the EEG? *Clin EEG Neurosci*. 2009;40(3):146-149. doi:10.1177/155005940904000305
48. Uhlhaas PJ, Singer W. Abnormal neural oscillations and synchrony in schizophrenia. *Nat Rev Neurosci*. 2010;11(2):100-113. doi:10.1038/nrn2774
49. Kishi T, Ikuta T, Sakuma K, et al. Theta burst stimulation protocols for schizophrenia: a systematic review and network meta-analysis. *JAMA Netw Open*. 2024;7(10):e2441159. doi:10.1001/jamanetworkopen.2024.41159
50. Raabe FJ, Galinski S, Papiol S, Falkai PG, Schmitt A, Rossner MJ. Studying and modulating schizophrenia-associated dysfunctions of oligodendrocytes with patient-specific cell systems. *NPJ Schizophr*. 2018;4(1):23. doi:10.1038/s41537-018-0066-4
51. Feinberg I. Schizophrenia: caused by a fault in programmed synaptic elimination during adolescence? *J Psychiatry Res*. 1982;17(4):319-334. doi:10.1016/0022-3956(82)90038-3
52. Duncan LE, Li T, Salem M, et al. Mapping the cellular etiology of schizophrenia and complex brain phenotypes. *Nat Neurosci*. 2025;28(2):248-258. doi:10.1038/s41593-024-01834-w
53. Ling E, Nemes J, Goldman M, et al. A concerted neuron-astrocyte program declines in ageing and schizophrenia. *Nature*. 2024;627(8004):604-611. doi:10.1038/s41586-024-07109-5
54. Windrem MS, Osipovitch M, Liu Z, et al. Human iPSC glial mouse chimeras reveal glial contributions to schizophrenia. *Cell Stem Cell*. 2017;21(2):195-208.e6. doi:10.1016/j.stem.2017.06.012
55. Chang MH, Waldeck JB, Stephan M, et al. iPSC-modelling reveals genetic associations and morphological alterations of oligodendrocytes in schizophrenia. *Transl Psychiatry*. 2025;15(1):287. doi:10.1038/s41398-025-03509-x
56. Lewis DA, Curley AA, Glausier JR, Volk DW. Cortical parvalbumin interneurons and cognitive dysfunction in schizophrenia. *Trends Neurosci*. 2012;35(1):57-67. doi:10.1016/j.tins.2011.10.004
57. Brown AS. The environment and susceptibility to schizophrenia. *Prog Neurobiol*. 2011;93(1):23-58. doi:10.1016/j.pneurobio.2010.09.003